



## Comparison of K-doped and pure cold-rolled tungsten sheets: Tensile properties and brittle-to-ductile transition temperatures



Philipp Lied<sup>a,\*</sup>, Wolfgang Pantleon<sup>b</sup>, Carsten Bonnekoh<sup>a</sup>, Simon Bonk<sup>a</sup>, Andreas Hoffmann<sup>c</sup>, Jens Reiser<sup>a,d</sup>, Michael Rieth<sup>a</sup>

<sup>a</sup> Karlsruhe Institute of Technology, Institute for Applied Materials – Applied Materials Physics, 76344, Eggenstein-Leopoldshafen, Germany

<sup>b</sup> Technical University of Denmark, Department of Mechanical Engineering, Section of Materials and Surface Engineering, 2800, Kongens Lyngby, Denmark

<sup>c</sup> PLANSEE SE, 6600, Reutte, Austria

<sup>d</sup> Precitec GmbH & Co. KG, 76571, Gaggenau, Germany

### ARTICLE INFO

#### Article history:

Received 27 March 2020

Revised 16 October 2020

Accepted 7 November 2020

Available online 13 November 2020

#### Keywords:

Cold-rolling

Potassium-doping

Recrystallization inhibition

Fracture toughness

Tensile strength

Hall-Petch relation

### ABSTRACT

For high-temperature environments, as in future fusion reactors, the use of tungsten materials has been sincerely discussed in the last decade. Although severe cold-rolling of tungsten leads to significant improvements in mechanical properties, the fine-grained microstructure of such tungsten material has to be stabilized. For that, the use of potassium-doping (K-doping) in tungsten sheets is investigated in our ongoing study. In this work, we compare mechanical properties of warm- and cold-rolled sheets of pure tungsten and K-doped tungsten (for five different degree of deformation respectively) by means of fracture toughness tests and tensile tests.

Fracture toughness and brittle-to-ductile transition temperatures ( $T_{BDT}$ ) are assessed, showing a slightly lower transition temperature for the cold-rolled K-doped sheets (lower than  $-100$  °C for the  $50$   $\mu\text{m}$  thick foil). The better performance of the K-doped sheet is related to its finer grain size. The thickest K-doped sheet shows a much higher  $T_{BDT}$  than its pure tungsten counterpart. This is presumably caused by the presence of several tens of micrometre thick bands, containing only low angle boundaries, in the microstructure of the K-doped sheet.

Tensile tests reveal an outstanding yield strength of  $2860$  MPa and an ultimate tensile strength of  $2970$  MPa for the thinnest K-doped sheet with similar, but slightly lower values for the pure tungsten counterpart. Both thinnest sheets show a drastic increase in ultimate tensile strength in correlation to their mean grain size, much higher than expected by a Hall-Petch relation. This deviation has been observed for the microhardness as well and is assumed to be caused by an extraordinary increase in the density of dislocations.

Our results indicate that no disadvantages in tensile strength and brittle-to-ductile transition are to be expected compared to pure tungsten, when K-doped tungsten is used to inhibit recrystallization in high-temperature environments.

© 2020 The Authors. Published by Elsevier B.V.

This is an open access article under the CC BY license (<http://creativecommons.org/licenses/by/4.0/>)

\* Corresponding author: Philipp Lied, Karlsruhe Institute of Technology, Institute for Applied Materials – Applied Materials Physics, 76344, Eggenstein-Leopoldshafen, Germany

E-mail addresses: [philipp.lied@kit.edu](mailto:philipp.lied@kit.edu) (P. Lied), [pawo@dtu.dk](mailto:pawo@dtu.dk) (W. Pantleon), [carsten.bonnekoh@kit.edu](mailto:carsten.bonnekoh@kit.edu) (C. Bonnekoh), [simon.bonk@kit.edu](mailto:simon.bonk@kit.edu) (S. Bonk), [andreas.hoffmann@plansee.com](mailto:andreas.hoffmann@plansee.com) (A. Hoffmann), [j.reiser@precitec.de](mailto:j.reiser@precitec.de) (J. Reiser), [michael.rieth@kit.edu](mailto:michael.rieth@kit.edu) (M. Rieth).

### Introduction

The use of tungsten (W) and tungsten-based materials in future fusion power reactors has been investigated and discussed for several years [1]. Tungsten is the element with the highest melting temperature among all metals ( $T_m = 3693$  K [2]), therefore it possesses a low vapour pressure in the plasma chamber of a fusion reactor. It exhibits a high wear resistance, as well as good high-temperature strength and good thermal conductivity. It is therefore considered as the most promising material for the use in critical parts of fusion reactors which have to suffer high thermal loads.

However, a major drawback of conventionally produced tungsten is its brittleness at room temperature. In order to avoid this disadvantage, the influence of cold-working on tungsten has been assessed in several studies [3–7]; mechanical properties like tensile properties [8,9] and fracture toughness [7,10] have been investigated in-depth on such severely rolled sheets. Such thin cold-rolled tungsten sheets could be joined to a laminate bulk material [11] or laminate pipes [12] for applications in fusion related environments.

On the other hand, the improvement of mechanical properties by severe deformation (e.g. rolling) also introduces higher driving forces for recovery and recrystallization [13], leading very likely to accelerated embrittlement during thermal treatment [14]. In order to reduce the tendency of recrystallization during the lifetime of the material in the reactor (by inhibiting the movement of grain boundaries), the incorporation of particles or precipitations into the material matrix is a well-established approach, such as carbides [15–18], oxides [19,20], or doping e.g. with potassium (K) which forms bubbles in the W matrix [21,22].

For example, extruded W-1%La<sub>2</sub>O<sub>3</sub> has been investigated, but a higher brittle-to-ductile transition temperature ( $T_{BDT}$ ) was found due to the presence of elongated La<sub>2</sub>O<sub>3</sub> particles in the rolled W matrix [23]. Another observation was the limited workability of W-1%La<sub>2</sub>O<sub>3</sub> in rolling studies. When approaching a specific degree of deformation in own experiments (April 2019), cracking along the rolling direction occurred, presumably by a preferred crack path along the elongated La<sub>2</sub>O<sub>3</sub> particles in W.

A very interesting approach is the incorporation of rhenium, in some studies also combined with K-doping [24]. The addition of several percent of rhenium significantly decreases the  $T_{BDT}$  and improves high-temperature strength with some drawbacks, e.g. lower thermal conductivity, higher irradiation embrittlement in peculiar irradiation conditions and increased bulk material costs compared to pure W [1,15,24,25].

Another approach is K-doping of tungsten. K-doping has been used for enhancing the creep properties of tungsten wires in tungsten filaments for many decades in the lighting industry. Recently, K-doped tungsten wires gained interest as well for fusion related materials in fibre-reinforced composites [26–28], and K-doping of hot-rolled tungsten plates together with rhenium addition has been investigated [24,29].

Combining heavy cold-rolling of tungsten sheets with K-doping – as used in the present study – is a new approach. Two sets of sheets with pure W and K-doped W (containing 60 ppm potassium) have been produced in the same manner with an increasing degree of deformation by rolling for direct comparison of the recrystallization behaviour and mechanical properties. Both sets of materials were characterized after rolling regarding their microstructural properties (grain size, rolling texture) and microhardness in the as-rolled condition. Despite a slight hardening effect by the K-doping, both materials showed similar results [30]. Additionally, isochronal annealing experiments were carried out, indicating a better performance in recrystallization inhibition with increasing degree of deformation for the K-doped W which retains a finer microstructure than pure W at temperatures above 1400 °C [30].

With these promising results in the recrystallization behaviour, the focus of further investigations shifted towards the mechanical properties of the rolled W sheets with the following questions in mind: Are mechanical disadvantages or even advantages to be expected, if pure W is replaced by K-doped W? K-doping seems to improve the hardness slightly [30]; does K-doping also have an impact on tensile strength? Are the severely rolled, K-doped sheets more brittle than pure W sheets, as seen e.g. for W-1%La<sub>2</sub>O<sub>3</sub> [23], or less, as Charpy-impact tests on 7 mm thick, K-doped plates indicate [31]? These open questions are assessed in this study by tensile and fracture toughness tests. After a materials and meth-

ods section, the results are presented for both testing procedures and are discussed separately afterwards in relation to results from the preceding study on microstructure and microhardness (as measured in sections defined by the rolling and the normal direction) [30].

## Materials and methods

### Materials

For this study, we used the same material sets as in a former rolling study [30]. These material sets have been produced from two sintered ingots at PLANSEE SE (Reutte, Austria): (i) K-doped tungsten, which is commercially available as “WVM”, and (ii) technically pure tungsten (> 99.97 wt.% W), which is also commercially available. The abbreviations for both materials used in this study (as in the previous one) are  $W_K$  and  $W_{\text{pure}}$ , respectively. Chemical analysis revealed a K-content of 60 ppm for  $W_K$  and technical purity for  $W_{\text{pure}}$  (the exact chemical compositions are given in [30]). Although pure tungsten and K-doped tungsten are commercially available, the rolling to very high degrees of deformation is a rather new approach [32] and has been advanced in our preceding study [30] to sheets of 50 µm thickness (thickness reduction more than 99%).

The rolling study involved three major processing steps, beginning with hot-rolling above the standard recrystallization temperature of 1250 °C to shape the sintered ingot to a 5 mm thick sheet. The subsequent warm-rolling was performed in the range between 800 °C and 1000 °C with intermediate heating steps. After a thickness reduction of around 80% (logarithmic strain of 1.6), one part of the resulting sheet was separated as first sheet  $W_K(1.6)$  of the series. After that, the warm-rolling process was continued and the sheets  $W_K(2.7)$  and  $W_K(3.1)$  at logarithmic strains of 2.7 and 3.1 were separated likewise. In the last production steps, the rolling temperature was reduced below 300 °C and  $W_K(3.7)$  as well as  $W_K(4.6)$  were produced by cold-rolling to logarithmic strains of 3.7 and 4.6. In this way, we produced  $W_K$  sheets of the same chemical composition with five different degrees of deformation. The same procedure was applied to  $W_{\text{pure}}$ , to create sheets with comparable logarithmic strain ( $\epsilon_{\log}$ ):  $W_{\text{pure}}(1.6)$ ,  $W_{\text{pure}}(2.7)$ ,  $W_{\text{pure}}(3.3)$ ,  $W_{\text{pure}}(3.7)$  and  $W_{\text{pure}}(4.7)$ . An overview of the resulting thicknesses and the corresponding engineering strains ( $\epsilon_{\text{eng}}$ ) is given in Table 1. For convenience, the results of grain size determination from EBSD data [30] are included in the table.

### Fracture toughness tests

For fracture toughness tests, single edge notched tensile (SENT) specimens were prepared from the manufactured sheets listed in Table 1 ( $W_K(1.6)$  to  $W_K(4.6)$  and  $W_{\text{pure}}(1.6)$  to  $W_{\text{pure}}(4.6)$ ). Cutting of these specimens (contour and crack-starting notch) was done by means of electrical discharge machining. The sample thickness corresponded to the thickness of the respective sheet, which ensures that microstructure heterogeneities, as reported in the preceding study [30] on the investigated sheets or through-thickness gradients as observed in rolled sheets from the surfaces in contact with the rolls [33], are reflected in the mechanical properties as well, since the whole specimen width is tested. With the crack-starting notch along the transversal direction, the testing procedure in this study loads the L-T crack system as described in ASTM E399 [34]. The notch length ( $a$ ) is chosen as half of the specimen width ( $w$ ).

A fatigue pre-crack was not inserted in the specimen (which is common practice for brittle materials), as this would have required a disproportional experimental effort for more than 110 tested samples. Preparing notches by FIB, as used in similar studies on thin tungsten sheets [10], would not have been possible

**Table 1**

Comparison of the initial hot-rolled plate (HR) and the investigated warm-rolled (WR) and cold-rolled (CR) W sheets by thickness ( $t$ ), engineering and logarithmic strain ( $\epsilon$ ). Average grain sizes, as analysed in the previous study [30], were determined by measuring the length between line intercepts along normal direction (ND) with high angle boundaries (HABs), as well as all types of boundaries, including low angle boundaries (LABs). Ratios between measuring length ( $L_0$ ) in tensile tests and (square root of) cross section area of used samples ( $A_0$ ) are given in the last column.

| Material   | Rolling | $t$ / mm | $\epsilon_{eng}$ / % | $\epsilon_{log}$ / - | $d_{ND}(HAB)$ / $\mu\text{m}$ | $d_{ND}(HAB+LAB)$ / $\mu\text{m}$ | $L_0/A_0^{1/2}$ / - |
|------------|---------|----------|----------------------|----------------------|-------------------------------|-----------------------------------|---------------------|
| W, K-doped | HR      | 5.0      | 0.0                  | 0.0                  | -                             | -                                 | -                   |
| W, K-doped | WR      | 1.03     | 79.4                 | 1.6                  | 1.87                          | 0.48                              | 9.1                 |
| W, K-doped | WR      | 0.35     | 93.0                 | 2.7                  | 0.63                          | 0.34                              | 15.5                |
| W, K-doped | WR      | 0.22     | 95.6                 | 3.1                  | 0.45                          | 0.27                              | 19.6                |
| W, K-doped | CR      | 0.127    | 97.5                 | 3.7                  | 0.26                          | 0.16                              | 25.8                |
| W, K-doped | CR      | 0.052    | 99.0                 | 4.6                  | 0.17                          | 0.11                              | 21.7                |
| W, pure    | HR      | 5.4      | 0.0                  | 0.0                  | -                             | -                                 | -                   |
| W, pure    | WR      | 1.09     | 79.8                 | 1.6                  | 0.80                          | 0.40                              | 8.8                 |
| W, pure    | WR      | 0.36     | 93.3                 | 2.7                  | 0.46                          | 0.32                              | 15.3                |
| W, pure    | WR      | 0.19     | 96.5                 | 3.3                  | 0.43                          | 0.30                              | 21.1                |
| W, pure    | CR      | 0.134    | 97.5                 | 3.7                  | 0.30                          | 0.20                              | 25.1                |
| W, pure    | CR      | 0.051    | 99.1                 | 4.7                  | 0.17                          | 0.11                              | 21.9                |

with thicker specimen up to 1 mm thickness. Therefore, crack-starting notches were prepared by EDM as they contain multiple thermally induced cracks in the surface (see [7,35] and references therein). In this manner, the fracture toughness could be overestimated and the BDTT underestimated, which should be kept in mind when comparing the presented values to other studies. Nevertheless, this study aims mainly to compare similarly produced pure and K-doped W sheets of varying degree of deformation and the values obtained here are comparable to each other and to values from similar studies using the same notching method [7,35].

A Zwick-Roell 1474 universal testing machine (electromechanical test device with a screw-driven step-motor), equipped with an Instron SFL 3119-400 series environmental chamber, was used for all low and intermediate temperature tests, i.e. between  $-150$  °C and  $320$  °C). All tests are conducted in air as no oxidation is to be expected in this temperature regime. Cooling in the chamber was achieved with inlet of liquid nitrogen. SENT specimens were loaded in tension in mode I with a fixed velocity of the crosshead of the testing machine. Depending on the sample thickness, the velocity was adjusted to achieve an applied loading rate ( $dK/dt$ ) in the elastic regime of  $1 \text{ MPa m}^{0.5} \text{ s}^{-1}$  for all tests.

From the resulting force ( $F$ ) versus displacement ( $u$ ) curve, the critical force ( $F_Q$ ) is calculated as described in ASTM E399 [34]: A secant is applied to the  $F$ - $u$  curve with 95% of the slope of the linear elastic part and the upper intersection point of this secant with the  $F$ - $u$  curve is taken as  $F_Q$ . The sample is classified as ductile if the  $F$ - $u$  curve shows a clear peak with a drop in force before fracture (excluding pop-in events). Semi-brittle sample behaviour was identified if the curve does not show a distinct drop and fractures in the regime where plastic deformation begins to dominate the curve. In this case, the secant with 95% of the slope still intersects with the  $F$ - $u$  curve. If the secant does not intersect the  $F$ - $u$  curve, the sample is classified as brittle in the respective testing condition and the maximum force before fracture is taken as  $F_Q$ . The fracture toughness ( $K_Q$ ) is calculated from  $F_Q$  as

$$K_Q = \frac{F_Q}{w t} \sqrt{\pi a} f\left(\frac{a}{W}\right) \quad (1)$$

with thickness ( $t$ ) and width ( $w$ ) of the specimen, as well as length of the crack-starting notch ( $a$ ) and  $f(a/w)$  as correction factor, compensating for the finite size of the specimen [34]. In this study, a value of 2.85 has been chosen for the correction factor  $f(a/w)$  from Murakami's tables [36], as fitting for a ratio of 0.5 for  $a/w$ . Note, that Eq. (1) takes into account the different specimen thickness ( $t$ ), but for the thin samples, plain strain conditions cannot be ensured. Therefore, the measurements do not meet the require-

ments for calculation of plain strain fracture toughness ( $K_{IC}$ ) as specified by ASTM 399 [34] and the fracture toughness value ( $K_Q$ ) reported here must be comprehended as a geometry-dependent value which provides overestimated values of the fracture toughness. This geometry-dependent value cannot be compared directly for sheets with different thicknesses. Nevertheless, this does not exclude a comparison of the fracture toughness of pure W and K-doped sheets with identical rolling deformation.

For more details on the testing procedure and data evaluation, as well as the classification of brittle, semi-brittle and ductile behaviour, we refer to an earlier study [7] which was conducted in the same manner.

#### Tensile tests

For tensile tests, flat, bone-shaped specimens have been prepared out of the manufactured sheets by electrical discharge machining. The gauge section of the specimens, where the elongation was measured by an extensometer, had a width of 2 mm and a length of 14.1 mm. The sample thickness corresponded to the thickness of the respective sheet. All samples were cut from the rolled sheets along the rolling direction, so that the tensile direction lies parallel to the rolling direction. The specimen surface was neither ground nor polished, so that the surface exhibits the original surface roughness after rolling and the surface quality after EDM along the edges.

Tensile tests were performed with a universal mechanical testing machine (Zwick-Roell Z150, Germany) equipped with a vacuum high-temperature radiation heater (MAYTEC Mess- und Regeltechnik, Germany). This electro-mechanical test device is driven by screw-based transmission, propelled by a step-motor. All tests were carried out with a strain rate of  $10^{-3} \text{ s}^{-1}$  in displacement-controlled mode. To test at different temperatures ( $T_t$ ) ranging from  $20$  °C to  $800$  °C, a special holder was designed (as used in [9]), in which the samples can be heated by a surrounding radiation heater before testing, without preloading or bending the sheets. It further enabled the use of an extensometer to measure the elongation directly on the sample, which yields much more precise strain measurements than the crosshead motion since the elongation of the testing device does not affect the measurement. By that, the measuring length ( $L_0$ ) for measuring the elongation on the sample was 13 mm, except for the thinnest sheets of  $50 \mu\text{m}$  thickness. Due to otherwise unacceptable bending of the thinnest samples,  $L_0$  had to be reduced to 7 mm. Decreasing ratios of measuring length to the (square root of the) area of the cross section ( $A_0$ ) (by thicker samples or increasing gauge length) can lead to a higher total elon-

gation. Even keeping constant ratios will not eliminate potential differences between the different specimen thicknesses, and hence the reported total elongations should be generally taken with caution, as specified in ASTM E8/E8M [37]. For comprehensiveness, we specify  $L_0/A_0^{1/2}$  ratios in Table 1.

For measurement at elevated temperatures, the samples were heated to the respective test temperature (300, 400, 600 or 800 °C) in the testing machine. Although the samples reached  $T_t$  during heating after around 15 min,  $T_t$  was kept for 45 min more before tensile testing, in order to ensure a uniform temperature distribution over the whole sample. Then, 1 h after starting of the heating procedure, tensile testing was performed.

During data evaluation, the ultimate tensile strength (UTS) is deduced from the maximum in the engineering stress ( $\sigma$ ) versus engineering strain ( $\varepsilon$ ) curve. The yield strength ( $\sigma_{ys}$ ) is deduced as proof stress after 0.2% plastic deformation from the intersection point of the stress-strain curve with a parallel line with the slope of the elastic part, shifted by 0.2% of strain [38]. An example of UTS and  $\sigma_{ys}$  analysis from stress-strain curves is shown in Fig. 2 for the sheets with 50  $\mu\text{m}$  thickness.

## Results

### Fracture toughness tests

The values for the (provisional) fracture toughness ( $K_Q$ ) obtained for  $W_{\text{pure}}$  and  $W_K$  are shown in Fig. 1. With increasing degree of deformation, an increase of the measured  $K_Q$  of ductile and semi-brittle fractured samples can be seen. The highest toughness value is recorded for the thinnest W sheet  $W_{\text{pure}}(4.7)$  with up to 140  $\text{MPa m}^{0.5}$ , compared to the next thicker sheet  $W_{\text{pure}}(3.7)$  with up to 60  $\text{MPa m}^{0.5}$ . The fracture toughness for sheets of  $W_K$  are in the same range.

Although the statistical support of the data is not as high as in a preceding study on similarly rolled W sheets [7], this study gives a rough estimation of the  $T_{\text{BDT}}$  for the investigated W sheets. For each W sheet, the brittle-to-ductile transition temperature ( $T_{\text{BDT}}$ ) is estimated by defining its lower limit by the brittle data point at the highest temperature. Its upper limit is defined by the next semi-brittle data point towards higher temperatures (or ductile data point if no semi-brittle data point is present). The resulting temperature range for the estimated  $T_{\text{BDT}}$  is marked by vertical bars in Fig. 1 for each sheet.

While  $W_{\text{pure}}(1.6)$  shows a low  $T_{\text{BDT}}$  between +20 °C to +50 °C, the  $T_{\text{BDT}}$  defined in this manner is not altered significantly for the warm-rolled sheets  $W_{\text{pure}}(2.7)$  and  $W_{\text{pure}}(3.3)$ . However, the cold-rolled sheets show a severe decrease of the  $T_{\text{BDT}}$  below room temperature at -50 °C to -60 °C for  $W_{\text{pure}}(3.7)$  and -80 °C to -100 °C for  $W_{\text{pure}}(4.7)$ .

The K-doped sheets show a similar trend, however,  $W_K(1.6)$  shows a much higher  $T_{\text{BDT}}$  between 240 °C to 260 °C than its  $W_{\text{pure}}$  counterpart. The  $T_{\text{BDT}}$  of  $W_K(2.7)$  and  $W_K(3.1)$  is comparable to that of their  $W_{\text{pure}}$  counterparts. The cold-rolled sheets  $W_K(3.7)$  and  $W_K(4.6)$  exhibit even a slightly lower  $T_{\text{BDT}}$  than  $W_{\text{pure}}(3.7)$  and  $W_{\text{pure}}(4.7)$  with -70 °C to -80 °C and -100 °C to -130 °C respectively.

### Tensile tests

The resulting engineering stress-strain ( $\sigma$ - $\varepsilon$ ) curves from the tensile tests at 20 °C are shown in Fig. 2. The curves reveal the lowest strength for the thickest tungsten sheets with even brittle behaviour for the  $W_K(1.6)$  sheet (therefore, no value for yield strength is deduced at 20 °C for this sheet). Ultimate tensile strength (UTS) and yield strength ( $\sigma_{ys}$ ) increase for both material

sets with increasing degree of deformation, with the sole exception of the transition from  $W_{\text{pure}}(2.7)$  to  $W_{\text{pure}}(3.3)$  where UTS is not increasing. The most significant increase by rolling is seen for the thinnest cold-rolled sheets compared to the next thicker sheets with thickness of 130  $\mu\text{m}$ :  $W_{\text{pure}}(4.7)$ , with a UTS of 2790 MPa, exhibits an increase of 700 MPa compared to  $W_{\text{pure}}(3.7)$  and  $W_K(4.6)$ , with a UTS of 2966 MPa, exhibits an increase of 800 MPa compared to  $W_K(3.7)$ .

The  $\sigma$ - $\varepsilon$  curves show a near elastic-ideal-plastic behaviour with a narrow hardening region, where plastic behaviour begins to dominate, and a long, flat plateau, indicating no recognizable necking of the samples during elongation up to several percent of strain. Although  $W_K(3.1)$  and  $W_K(3.7)$  show a slightly higher total elongation than their  $W_{\text{pure}}$  counterparts, the other  $W_K$  sheets show smaller total elongation compared to  $W_{\text{pure}}$ . Especially the cold-rolled  $W_K(4.6)$  has significantly less total elongation than  $W_{\text{pure}}(4.7)$ . As already mentioned,  $W_K(1.6)$  showed brittle behaviour, while  $W_{\text{pure}}(1.6)$  has the highest total elongation of all tested sheets (with 4.3%).

We further investigated both material sets by tensile tests at elevated temperatures (300 °C, 400 °C, 600 °C, 800 °C) and inferred the respective ultimate tensile strength (UTS) as well as yield strength ( $\sigma_{ys}$ ) as shown in Fig. 3. The UTS decreases with increasing test temperature, still showing at 800 °C more than 840 MPa for the sheets with lowest degree of deformation and more than 1200 MPa for the sheets with highest degree of deformation. Values for the yield strength ( $\sigma_{ys}$ ) are in a similar range (approximately 100 to 300 MPa lower than UTS) and show the same trends as the UTS with a decrease in strength with increasing test temperatures.

When comparing sheets of both material sets with same degree of deformation, all investigated  $W_K$  samples show slightly higher values for both, UTS and  $\sigma_{ys}$ , compared to their  $W_{\text{pure}}$  counterparts. Values for the total elongation are in a similar range for the K-doped sheets  $W_K$  compared to their counterparts of pure tungsten  $W_{\text{pure}}$  of same thickness (not shown here).

## Discussion

### Fracture toughness

The thinnest sheets  $W_{\text{pure}}(4.7)$  and  $W_K(4.6)$  show a significantly decreased  $T_{\text{BDT}}$  with less than -80 °C (193 K) and -100 °C (173 K) respectively. This is an outstanding performance for a tungsten material and surpasses even the excellent  $T_{\text{BDT}}$  of cold-rolled pure W sheets ( $\varepsilon_{\text{log}} = 4.1$ ) with -65 °C (208 K), which was reported in a preceding study [7]. However, care should be taken when comparing these values with other studies where fatigue cracks were induced in the sample preparation, as our results for the estimated BDTT could be slightly underestimated due to the notch created by EDM.

Comparing the  $T_{\text{BDT}}$  of the  $W_K$  sheets directly with their  $W_{\text{pure}}$  counterparts, the cold-rolled sheets of K-doped tungsten (50 and 130  $\mu\text{m}$  thickness) seem to have a slightly lower  $T_{\text{BDT}}$  than the corresponding pure tungsten sheets. However, the most striking difference between both material sets is seen in the  $T_{\text{BDT}}$  of the thickest sheets  $W_K(1.6)$  and  $W_{\text{pure}}(1.6)$  with around +250  $\pm$  10 °C and +35  $\pm$  15 °C respectively. This is an impressive discrepancy between the  $T_{\text{BDT}}$  with  $\Delta T_{\text{BDT}}$  of more than 200 K. A reason for this could be the significant difference in the microstructure between both sheets, which has been elucidated in the previous study [30]: While both sheets show a weak rolling texture with preferred  $\alpha$ - and  $\gamma$ -fibre texture components and shear textures near the sheet surface, the sheet  $W_K(1.6)$  shows a peculiar phenomenon where bands of several tens of  $\mu\text{m}$  thickness along the normal direction dominate the microstructure in the centre of the longitudinal sec-

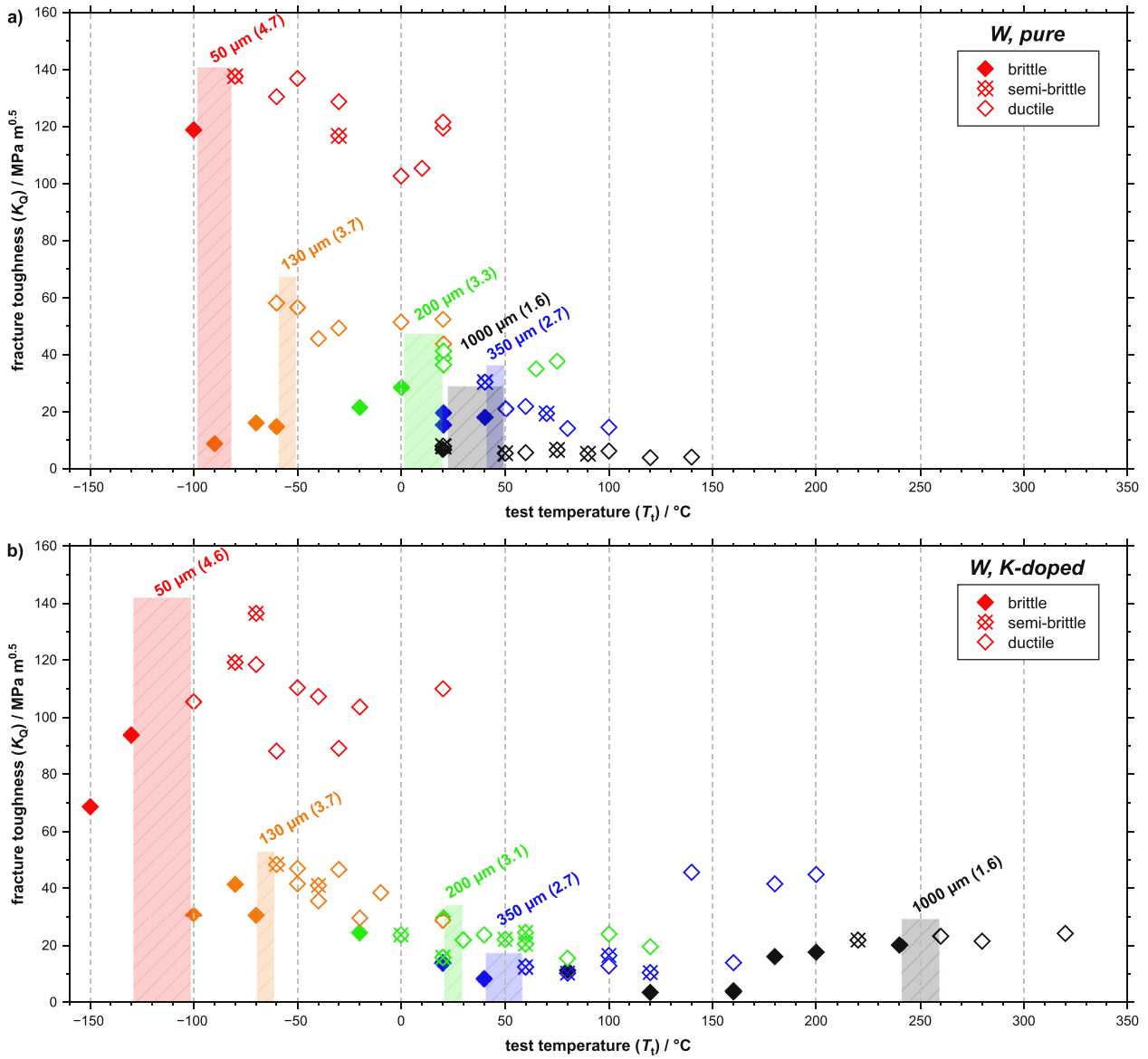


**Fig. 1.** Dependence of fracture toughness on test temperature for all sheets with five different degrees of deformation from (a)  $W_{\text{pure}}$  and (b)  $W_K$ . Fracture behaviour is classified as brittle (closed symbol), semi-brittle (crossed symbol) and ductile (open symbol); more details on the classification are given in the methods section. For each sheet, the estimated  $T_{BDT}$  between the data point at the highest temperature showing brittle fracture and the semi-brittle or ductile data point at the next higher temperature is marked by vertical bars for each sheet.

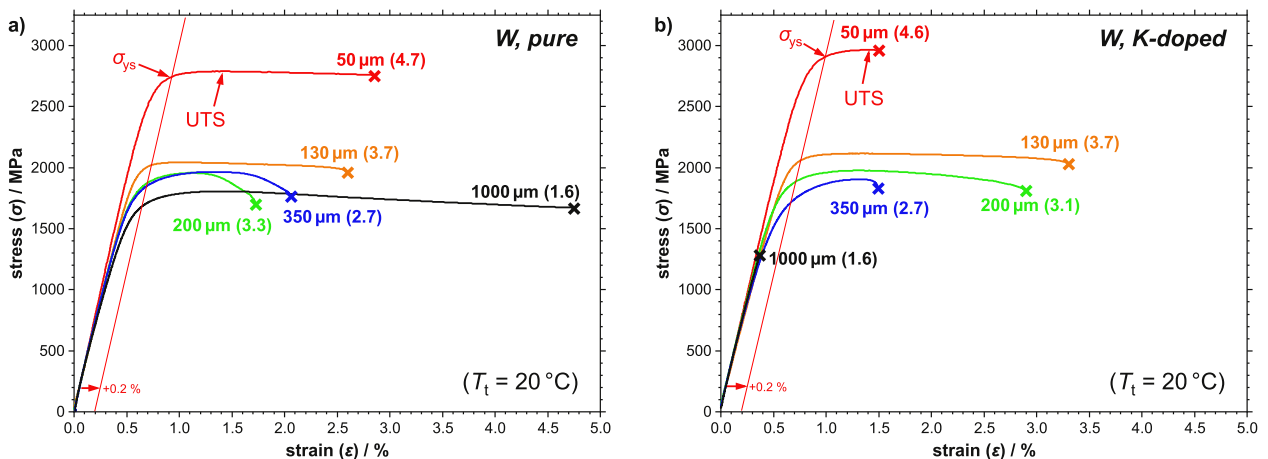


**Fig. 2.** Engineering stress-strain curves for (a) pure tungsten and (b) K-doped tungsten sheets at room temperature ( $20^{\circ}\text{C}$ ) for all sheets with five different degrees of deformation.

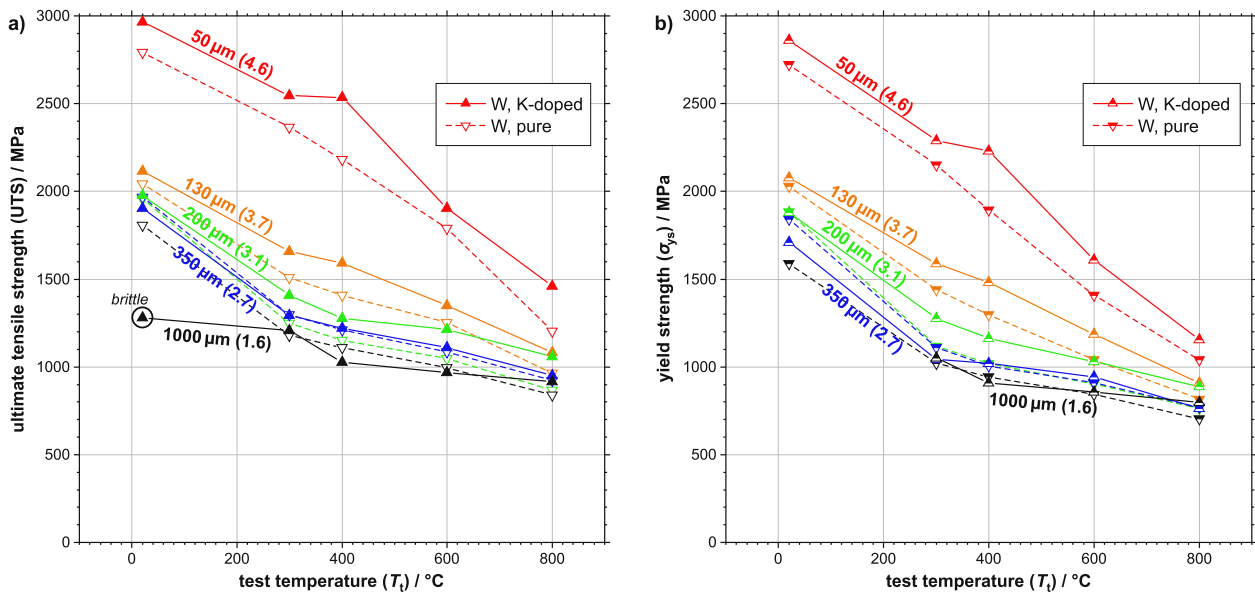


Fig. 3. Results on the tensile tests of pure and K-doped tungsten sheets: (a) ultimate tensile strength and (b) yield strength. The thickest K-doped sheet (1000 μm) showed brittle material behaviour in all tests at 20 °C (black circle), therefore its UTS is not directly comparable and no value for yield strength is deduced at this temperature.

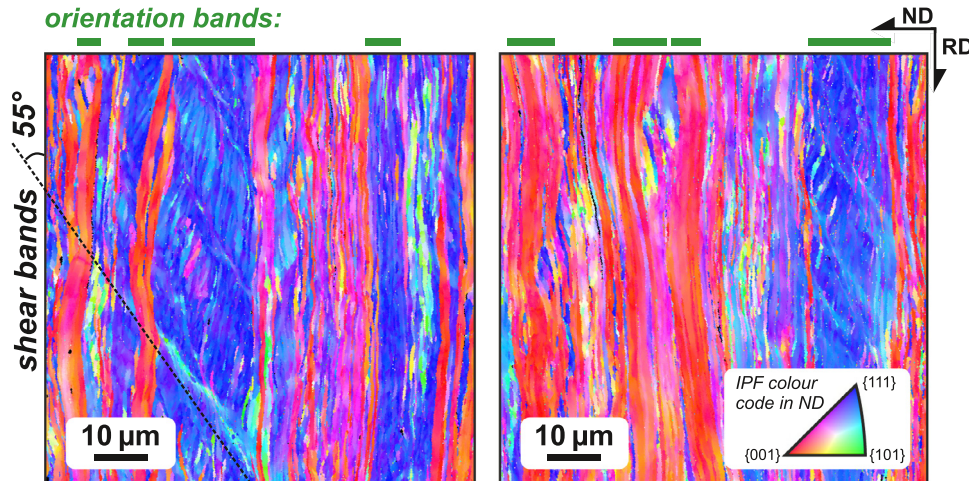


Fig. 4. Orientation maps of RD/ND sections of  $W_{K(1.6)}$ . Both sections show several micrometre thick bands (marked by green bars at the top), which do not contain HABs. They consist only of orientation components from either  $\alpha$ -fibre (appearing red to purple) or  $\gamma$ -fibre (appearing blue). Some of these orientation bands additionally contain shear bands, inclined by 55° to the rolling direction. For more detail, we refer to the preceding study [30].

tion (Fig. 4, or see Fig. 8 in [30]). These bands stretch along the rolling direction, contain only LABs and consist only of a single orientation component from  $\alpha$ - or  $\gamma$ -fibre. Therefore, the bands were referred to as “orientation bands” in the previous study. Some of these comprise shear bands, especially the orientation bands consisting only of crystallites with  $\gamma$ -fibre orientations. The possible influence of the orientation bands is discussed in the following.

The relationship of the  $T_{BDT}$  to the grain size has been investigated in literature for example for steels [39] and good correlations with the grain size by Hall-Petch relation have been found for tungsten sheets as well [3,14]. Similarly, we compared the dependence of  $T_{BDT}$  on grain size in this study with a Hall-Petch relation. Mean grain sizes have been determined by EBSD in the preceding study [30] as boundary spacing along normal direction  $d_{ND}$  (given in Table 1), and the estimated  $T_{BDT}$  is plotted against  $d_{ND}^{-1/2}$  in Fig. 5. As in the preceding study [30], two approaches are tested: First, only high angle boundaries with misorientation angles above 15° are considered in the boundary spacing  $d_{ND}(HAB)$ , second all boundaries with misorientation angles above 2° are con-

sidered in the boundary spacing  $d_{ND}(HAB+LAB)$ . While the first approach is commonly used, the second approach was pursued in the preceding study [30] due to the specific microstructure of the severely cold-rolled sheets with high densities of LABs. Since a linear regression of the Hall-Petch relation for microhardness in dependence on  $d_{ND}$  showed a far better fit to the data when LABs were included in  $d_{ND}$  (see Fig. 10 in [30]), a significant contribution of LABs to hardness has been discussed.

In a grain size analysis with line intercepts along ND, where only HABs are considered as grain boundaries, orientation bands appear as huge grains with several tens of μm thickness as they contain mainly LABs. Therefore, the mean grain size  $d_{ND}(HAB)$  has a large value for the sheet  $W_{K(1.6)}$ , which shows many orientation bands, compared to its counterpart  $W_{pure(1.6)}$  (Table 1). For the boundary spacing  $d_{ND}(HAB+LAB)$ , the discrepancy between both sheets is rather small.

These findings are also reflected in Fig. 5, where  $W_{K(1.6)}$  shows significantly smaller values for  $d_{ND}(HAB)^{-1/2}$  than  $W_{pure(1.6)}$ . The curve for the K-doped sheets shows a more or less linear decrease

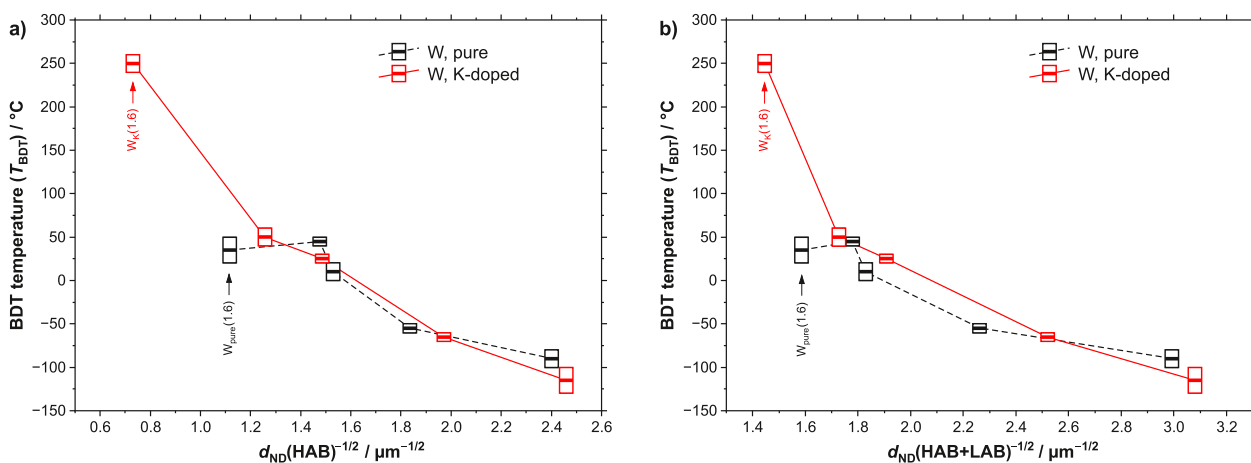


**Fig. 5.** Dependence of estimated brittle-to-ductile transition temperature on grain size  $d_{ND}$  for pure W and K-doped W. a) Only HABs are considered in  $d_{ND}(\text{HAB})$ . b) As an alternative approach, HABs and LABs are both considered in the boundary spacing  $d_{ND}(\text{HAB}+\text{LAB})$ . Vertical bars mark the lower and upper limit of  $T_{BDT}$  with the estimated  $T_{BDT}$  as data point in the middle between.

for  $T_{BDT}$  with increasing  $d_{ND}(\text{HAB})^{-1/2}$  for all degrees of deformation (Fig. 5a). If LABs are considered in  $d_{ND}$  (Fig. 5b), the curve still shows a linear decrease for the  $W_K$  sheets with higher degree of deformation only, but  $W_K(1.6)$  deviates from the linear behaviour. This indicates that the density of HABs is still controlling the  $T_{BDT}$  in contrast to microhardness which was controlled by both types of boundaries. The high amount of orientation bands causes a low density of HABs, leading to a higher  $T_{BDT}$  in  $W_K(1.6)$  compared to  $W_{\text{pure}}(1.6)$ .

It may be further argued, that crack propagation can proceed more easily across such an orientation band. In general, HABs at a crack front are known to be substantial sources for dislocations during plastic deformation [40]. Since the orientation bands solely contain LABs, the amount of dislocation sources would be drastically reduced. If the density of dislocation sources is insufficient during the deformation, such bands could be more prone to brittle fracture than a more fine-grained microstructure with higher density of dislocation sources. Therefore, orientation bands could represent regions in the sample, where cracking could propagate more easily. Due to the huge volume of the orientation bands, an induced crack could spread more easily through the sample volume and initiate cracking of the surrounding microstructure as well, therefore leading to a brittle fracture on a macroscopic scale. To confirm this hypothesis, investigations e.g. of the fracture surface could prove useful.

The reasons for the occurrence of the orientation bands in the  $W_K$  sheet remain unknown at the present stage. From experience of the manufacturer, K-doped W can develop huge grains during sintering at high temperatures due to abnormal grain growth. Abnormal grain growth could also occur during the hot rolling process through intermediate heating of the sheets. Additionally, abnormal grain growth – instead of normal grain growth – is known to be promoted by the presence of particles or bubbles, which are pinning grain boundaries and prevent normal grain growth [13,41], as observed in K-doped W [42,43]. Assuming a microstructure with abnormally large grains present in the sintered ingot or the hot-rolled plate, it is imaginable that an orientation band could originate from an abnormally large grain by deformation and elongation during rolling. However, this reasoning is speculative, as the occurrence of abnormally grown grains in the hot-rolled conditions has not been investigated in detail. Furthermore, it is unknown, if orientation bands can also develop in pure W sheets in general, although none of these have been found in the investigated pure W sheets which are used in this study [30]. Never-

theless, since our data suggest a brittle behaviour of the sheets by the existence of orientation bands in the 1 mm thick sheet, it seems advisable to avoid orientation bands in the final product, if possible. The data also imply that further rolling can reduce the effect of the orientation bands, as  $d_{ND}(\text{HAB})$  and  $T_{BDT}$  are drastically reduced in the next rolling step from  $W_K(1.6)$  to  $W_K(2.7)$  (Fig. 5).

Although pure W and K-doped W sheets are commercially available at PLANSEE, we want to emphasize that the tested materials in this study are part of a rolling study to investigate the evolution of microstructure and mechanical properties of two material classes and that most sheets represent intermediate stages in the rolling process. Therefore, especially the sheets with lower degree of deformation (which did not receive cold-rolling) do not represent standard commercially available materials from PLANSEE. The data presented here indicate that optimizations in the manufacturing should be considered, if phenomena like the orientation bands would persistently occur in future productions of 1 mm thick W sheets (with or without K-doping).

### Tensile tests

#### Comparison of W materials at room temperature

Nearly all sheets showed ductile behaviour in the tensile tests at 20 °C, except the brittle behaviour for the  $W_K(1.6)$  sheet. An elastic-ideal-plastic behaviour in the  $\sigma$ - $\varepsilon$  curves (Fig. 2) can be seen particularly well for the cold-rolled materials  $W_{\text{pure}}(3.7)$ ,  $W_{\text{pure}}(4.7)$  and  $W_K(3.7)$ . Such a phenomenon of near elastic-ideal-plastic behaviour has been described by Wei and Kecskes [44] and a previous study from Bonk et al. [9] for cold-rolled tungsten sheets with 100  $\mu\text{m}$  thickness ( $\varepsilon_{\text{log}} = 4.0$ ), similarly produced as the  $W_{\text{pure}}$  sheets in our own study.

Quite unique is the high amount of total elongation for  $W_{\text{pure}}(1.6)$  with 4.3% (Fig. 2) which increases to more than 6% for tensile tests above 300 °C. In an analogous study on pure tungsten sheets [9], for the thickest W sheet with similar degree of deformation as  $W_{\text{pure}}(1.6)$  the amount of total elongation is much lower (around 1.5%) at room temperature. However, beginning at a test temperature of 200 °C, this thickest W sheet also showed the highest total elongation of all investigated sheets with more than 5% [9]. As already mentioned in the methods section, decreasing  $L_0/A_0^{1/2}$  ratios can yield increasing total elongation, which could be the reason for the high elongation of  $W_{\text{pure}}(1.6)$  with the lowest  $L_0/A_0^{1/2}$  ratio (Table 1).

On the other hand, the K-doped counterpart  $W_K(1.6)$  is the only sheet showing brittle behaviour at room temperature. Even though tensile tests and fracture toughness tests are difficult to compare, the brittle behaviour during tensile testing corresponds to the results of the fracture toughness tests where  $W_K(1.6)$  shows the highest  $T_{BDT}$  of all sampled sheets, which is presumably caused by the high amount of orientation bands with tens of micrometres in thickness, as discussed before. As the samples are not polished, slight surface roughness by the rolling process can initiate cracks, leading to more brittle behaviour. This, however, should be equal among all investigated samples in this study.

The increasing UTS and  $\sigma_{ys}$  with increasing degree of deformation can be easily explained by the decreasing grain size. However, the very high tensile strength of the 50  $\mu\text{m}$  thick sheets (grain size  $\sim 0.17 \mu\text{m}$  along ND), with around 2790 MPa for  $W_{\text{pure}}(4.7)$  and 2970 MPa for  $W_K(4.6)$ , is outstanding and to our knowledge the highest UTS reported for a rolled tungsten sheet. This applies to  $\sigma_{ys}$  as well with values of 2720 MPa and 2860 MPa respectively. To put these results into perspective: These sheets are outperforming for example a pure W sheet with 100  $\mu\text{m}$  thickness (and lower degree of deformation) of the preceding study from [9] where values of around 2300 MPa for UTS and 2200 MPa for  $\sigma_{ys}$  have been observed (grain size of 0.24  $\mu\text{m}$ ). It should be kept in mind that this is an anisotropic material and tensile tests with loading along other directions should yield lower results.

For further comparison, many results on tensile tests for tungsten wires can be found in the literature. Naturally, wires can be produced with high degree of deformation more easily than rolled sheets. For the same logarithmic strain, grains develop much smaller sizes along TD in rolling than along the radial direction in wire drawing. Or other way round: The same grain sizes are achieved in wire drawing after much larger logarithmic strain than in rolling. Logarithmic strains of more than 8 are common for wires and by that, extreme UTS values of W wires can be found in reports, e.g. 5.2 GPa observed for wires with a radial grain size of 100 nm [21]. However, other studies report much lower UTS values for commercially available W wires. For example 2914 MPa to 2940 MPa for drawn wire of pure W (150  $\mu\text{m}$  diameter) with a radial grain size of 0.1  $\mu\text{m}$  to 1  $\mu\text{m}$  [45], or 2721 MPa for drawn wire of K-doped W (150  $\mu\text{m}$  diameter, grain size not mentioned) [28], both provided by OSRAM GmbH, Schwabmünchen. These lower UTS from commercially available wires compared to the reported 5.2 GPa can be caused by lower degree of deformation, but also from potential annealing for stress relieving. Due to thermal instability [30], degradation in strength by annealing above  $\sim 700 \text{ }^\circ\text{C}$  can be expected for the highly deformed sheets as well and has to be considered when dealing with elevated temperatures, as in a fusion reactor. While it is difficult to compare the mentioned values from wires with sheets since the grain shape is very different, from a technological point of view, it is quite interesting, from a technological point of view, that rolled sheets can reach a tensile strength similar to commercially available wires.

Coming back to rolled W sheets, another study [46] compared tensile properties of K-doped W (30 ppm K) and pure W plates, manufactured at A.L.M.T. by hot-rolling with 80% thickness reduction and following heat treatment (900  $^\circ\text{C}$  for 20 min). With a similar strain rate to our study ( $10^{-3} \text{ s}^{-1}$ ), the K-doped plate showed a  $\sigma_{ys}$  of around 1400 MPa at room temperature. The pure W plate showed brittle behaviour at room temperature, but ductile behaviour at and above 200  $^\circ\text{C}$ , with a  $\sigma_{ys}$  of around 750 MPa at 200  $^\circ\text{C}$  and even above 800 MPa for the K-doped plate at 200  $^\circ\text{C}$ . This difference between both materials, however, is not related directly to the effect of K-doping, but to the grain size, as the pure W sheet in [46] had a more coarse grained structure than the K-doped sheet. The authors suggest that more pronounced grain re-

finement is induced during rolling by K-addition. New data from our preceding study [30] however show that the grain size from  $W_K$  sheets does not decrease more severe than the grain size from  $W_{\text{pure}}$  sheets during cold-rolling, but only during warm-rolling (e.g. see Fig. 4 in [30]). The latter suggests that K-bubbles in the W sheet do not directly enhance grain refinement during rolling, but inhibit growth of grains during heating of the W sheets between the warm-rolling steps.

#### UTS and $\sigma_{ys}$ at elevated temperatures

A decreasing UTS and  $\sigma_{ys}$  are observed with increasing temperature (Fig. 3), as expected by the occurrence of thermally activated processes [47]. Regarding the dependence of the yield stress on temperature, the results are in line with the comparable tensile test campaign using only pure W sheets [9]. While the decreasing  $\sigma_{ys}$  is mainly caused by an increased mobility of dislocations with increasing temperature, the decrease in UTS is additionally influenced by enhanced annihilation of dislocations due to dynamic recovery. While the cold-rolled sheets with high degree of deformation seem to be more susceptible for dynamic recovery, the warm-rolled sheets, however, show a fairly limited decrease in UTS between 400  $^\circ\text{C}$  to 800  $^\circ\text{C}$ , indicating that dynamic recovery already occurred during warm-rolling.

As shown by isothermal annealing experiments, the microstructure (especially of the thinnest W sheets) starts to become unstable at around 700  $^\circ\text{C}$  [30]. Therefore, one should keep in mind that during tensile testing at 800  $^\circ\text{C}$ , where the sample is kept at the testing temperature  $T_t$  for around 45 min to guarantee a uniform temperature distribution before the actual tensile test, the thin W sheets are already starting to degrade their mechanical properties due to extended recovery [30].

#### Hall-Petch relation

To confirm that the increasing UTS and  $\sigma_{ys}$  with increasing degree of deformation is caused by the decreasing grain size (following a Hall-Petch relation), the UTS of all tensile tests from room temperature up to 800  $^\circ\text{C}$  is plotted in Fig. 6a. Except for the sheets with highest degree of deformation (and for sample  $W_K(1.6)$  which is brittle at room temperature), an increase in UTS with decreasing  $d_{\text{ND}}(\text{HAB})$  can be observed for all  $T_t$ . One deviation from this trend in UTS can be found between  $W_{\text{pure}}(2.7)$  and  $W_{\text{pure}}(3.3)$  (sheets marked in Fig. 6). As discussed in the preceding study [30], this pair of sheets showed no significant difference in grain size and in microhardness, despite that  $W_{\text{pure}}(3.3)$  has been separated from the 350  $\mu\text{m}$  thick  $W_{\text{pure}}(2.7)$  sheet and rolled further down to 200  $\mu\text{m}$  thickness. This effect could be caused by temporal variations in the warm-rolling process, e.g. slightly longer warming up times of  $W_{\text{pure}}$  between the warm-rolling steps and resulting restoration processes.

For the thinnest sheets  $W_K(4.6)$  and  $W_{\text{pure}}(4.7)$ , a severe increase in UTS can be seen in Fig. 6a. For comparison, in the preceding study [30] with the same materials, the dependence of the microhardness on grain size  $d_{\text{ND}}(\text{HAB})$  showed a significant deviation from the Hall-Petch relation as well, but for all four sheets treated by cold-rolling, namely  $W_K(3.7)$ ,  $W_{\text{pure}}(3.7)$ ,  $W_K(4.6)$  and  $W_{\text{pure}}(4.7)$ . With the alternative approach of inclusion of all types of boundaries in  $d_{\text{ND}}(\text{HAB}+\text{LAB})$ , the Hall-Petch relation was fitting for the cold-rolled sheets as well, except for  $W_K(4.6)$ , where the microhardness was still much higher than expected from a Hall-Petch relation. Such a deviation from the Hall-Petch relation with a much higher value than expected can be observed for the UTS as well, however only for both sheets with highest degree of deformation  $W_K(4.6)$  and  $W_{\text{pure}}(4.7)$  (Fig. 6a). Consideration of LAB in  $d_{\text{ND}}(\text{HAB}+\text{LAB})$  does not cure this deviation (Fig. 6b).

This raises the following questions: (1) Why do both sheets with highest degree of deformation have much higher UTS than

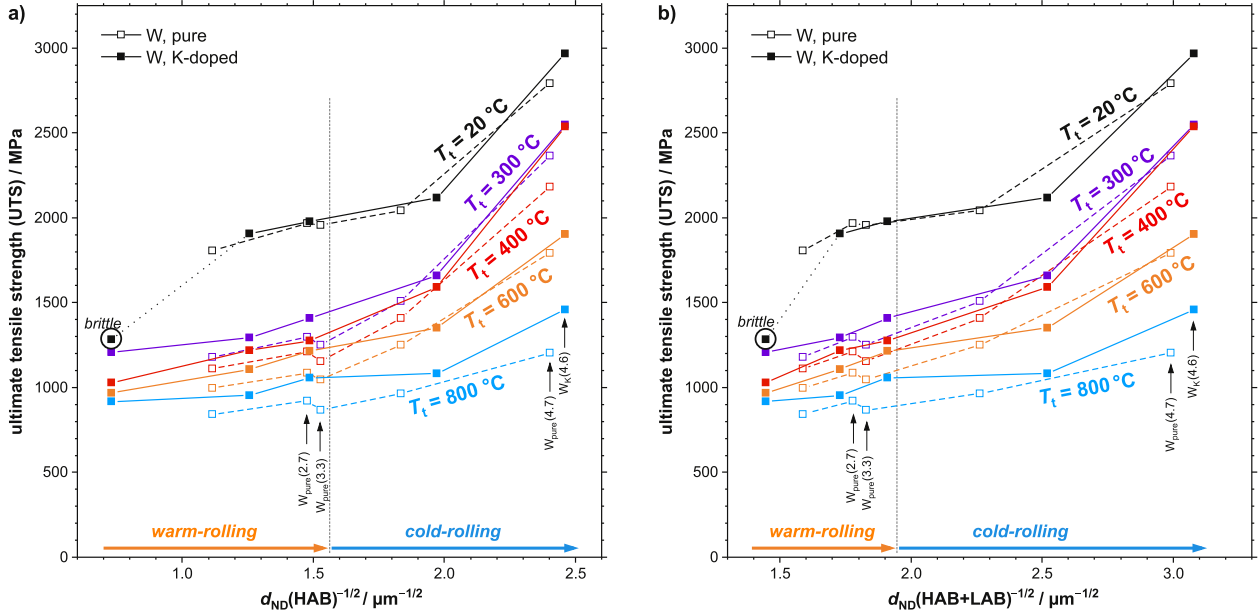


Fig. 6. Dependence of ultimate tensile strength on boundary spacing in normal direction ( $d_{ND}$ , see Table 1). a) Only HABs are considered as grain boundaries in  $d_{ND}(HAB)$ . b) All types of boundaries are included in the boundary spacing  $d_{ND}(HAB+LAB)$  as an alternative approach [30]. Shown are all data for tensile tests between test temperatures ( $T_t$ ) of 20 °C to 800 °C.

expected by the Hall-Petch relation? And (2) why does in case of microhardness only the sheet  $W_K(4.6)$  deviate from the Hall-Petch relation (see Fig. 10 in [30]), while for the UTS, both sheets  $W_K(4.6)$  and  $W_{pure}(4.7)$  deviate to much higher values (Fig. 6)?

For question (2), we repeated the microhardness measurements with two other samples for each respective sheet of  $W_K$  and  $W_{pure}$  in order to exclude systematic errors. All results consistently agreed to the previous measurement campaign, except the samples for  $W_{pure}(4.7)$ , where indeed a much higher hardness of  $754 \pm 11$  HV0.1 has been measured in the second test campaign on two samples, compared to the multiple measurements on the first sample, where a hardness of  $711 \pm 14$  HV0.1 has been determined before. As we can only speculate about the reasons for this difference, we took the new hardness value for  $W_{pure}(4.7)$  as a more realistic value, as the two new measurements showed similar values and the image is consistent when compared to the multiple tensile tests on this sheet: The new results of the microhardness for  $W_{pure}(4.7)$  are included in Fig. 7a, together with the UTS. UTS and microhardness are both much higher than expected by the Hall-Petch relation for both sheets  $W_K(4.6)$  and  $W_{pure}(4.7)$ . So in both cases microhardness and UTS of the two plates with highest degree of deformation showed large deviations from the Hall-Petch relation.

This leads back to question (1) about the reason for such a significant and non-linear increase of strength, but also of microhardness in the respective Hall-Petch relation (Fig. 7a). For the deviation in microhardness, it has been already discussed in [30] that the sample size is too small for conformity with DIN EN ISO 6507-1 [48] and that this could cause an apparent softer material behaviour as expected from the Hall-Petch relation. However, since we observe increased hardness values (and not a decrease as expected from surface effects), we can exclude an artefact caused by the small sample size to be the reason for such a deviation in hardness. The conjunction with the correspondingly enhanced UTS compared to the predictions of the Hall-Petch relation further proves that the trend for higher microhardness is an inherent material property and not an artefact. The determination of the boundary spacing  $d_{ND}(HAB+LAB)$  has to be considered as a potential source for the deviation as well. Rather small changes

in  $d_{ND}(HAB+LAB)$  can have a huge influence due to the reciprocal relationship, especially for small values of  $d_{ND}(HAB+LAB)$ . As discussed in the preceding study [30], the chosen step size of 40 nm for EBSD measurements is fairly at the limit to sufficiently resolve the small grain size of the sheets with highest degree of deformation. In order to exclude measurement errors, we reassessed the boundary spacing of  $W_K(4.6)$  by additional EBSD measurements with a step size of 10 nm. By that, the fractions of grains with smallest grain size below 40 nm were acquired sufficiently well. However, the resulting new value of  $95 \pm 2$  nm for  $d_{ND}(HAB+LAB)$  is by far not small enough in order to shift the data point of  $W_K(4.6)$  sufficiently to larger values (on the abscissa) and to gain a linear correlation in Fig. 7a. Additionally, the new value is within the standard deviation of the old value with  $105 \pm 10$  nm for  $d_{ND}(HAB+LAB)$ . Therefore, relevant errors in the measurement of  $d_{ND}(HAB+LAB)$  are considered highly unlikely.

In order to further assess the peculiar deviation of the thinnest W sheets in the Hall-Petch relation, we analysed the correlation between microhardness and UTS. A correlation between the elastic limit and Vickers hardness (HV) was established by [49]: Steel and copper samples were deformed by various amounts and thereafter Vickers hardness measurements performed. A representative elastic limit has been determined with around 8% of deformation, where a reasonable good proportionality was found between the Vickers hardness and the elastic limit with a proportionality factor (c) of around 2.9 to 3.0. Since the tungsten sheets in our study show only very low work-hardening and the UTS is reached already at 1% of deformation (Fig. 2), the UTS should correlate with HV as well in our case:

$$HV = c \text{ UTS} \quad (2)$$

However, this correlation should be seen more as a rule of thumb. If we use this simple Eq. (2) for our results with Vickers microhardness, we can find a good approximation for the sheets  $W_{pure}(1.6)$  to  $W_{pure}(3.7)$  and  $W_K(2.7)$  to  $W_K(3.7)$  with  $c = 3.1$  as correlation factor (Fig. 7b), similar as the values found in [49]. Again, the sheets with highest degree of deformation  $W_{pure}(4.7)$  and  $W_K(4.6)$  both show a deviation from the proportionality, with a greater increase in UTS (+400 MPa and +500 MPa respectively)

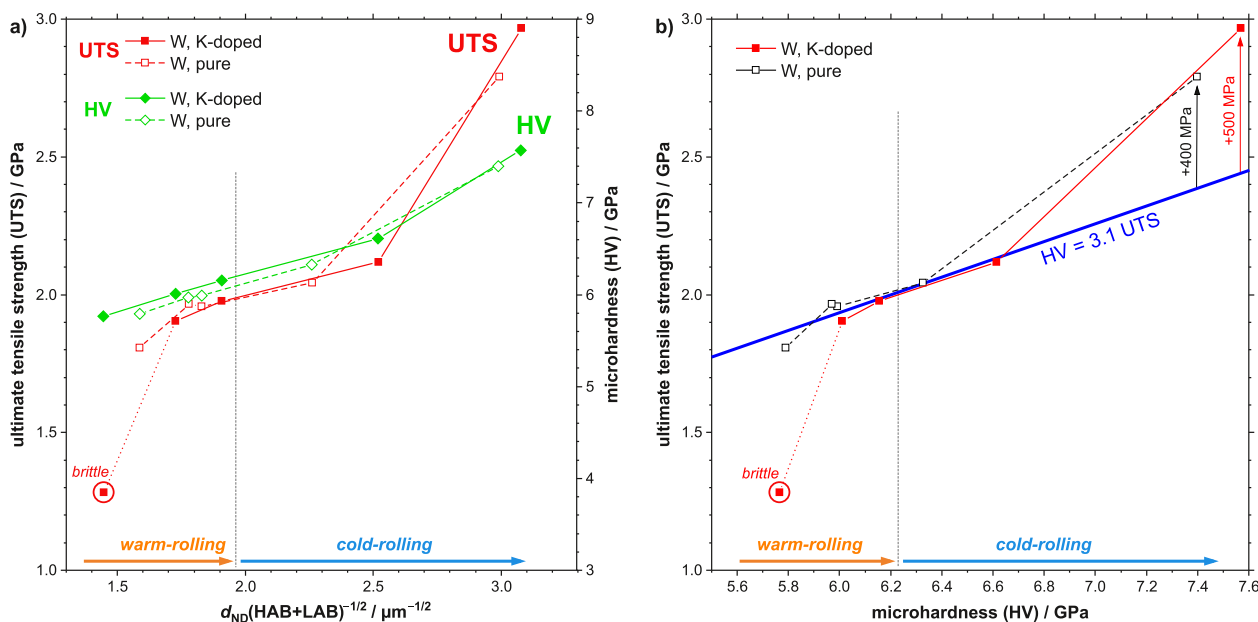


**Fig. 7.** a) Boundary spacing  $d_{ND}(HAB+LAB)$  in dependence on UTS at room temperature (red) and Vickers microhardness (green). Results of microhardness are included from [30] and the value of  $W_{pure}(4.7)$  has been revised through new measurements. b) UTS versus Vickers microhardness (HV). A fitted linear regression (blue line) showed a good approximation with a proportionality factor of  $c = 3.1$  relating UTS to microhardness (in GPa).

than predicted from microhardness in Eq. (2) (Fig. 7b). It has been argued in the preceding study [30] that the extraordinarily high hardness values for the thinnest sheets are valid, despite that the thicknesses of the thin sheets do not allow hardness measurements according to DIN EN ISO 6507-1 [48] and ASTM E92 [50] on sections defined by the rolling and the normal direction (the hardness indents with diagonal lengths of around  $17 \mu m$  are too large for the  $50 \mu m$  thin sheets exceeding the recommended ratio of 2.5 between distance from surface and diagonal length. For such a sample thickness, a maximum length of the diagonals of  $10 \mu m$  is recommended for the indent size. The too small foil thickness could result in lower hardness values than predicted from Hall-Petch compared to thicker sheets, but not in higher values as observed here (Fig. 7a). For both thinnest sheets, the observed lower hardness values *than predicted from their UTS values* (using  $c = 3.1$ , Fig. 7b) could be caused indeed by the small foil thickness and the real hardness could be even higher than the measured values of up to 771 HV0.1 (7.6 GPa) causing even larger deviations from the Hall-Petch relation.

Further care has to be taken, when comparing the determined proportionality factor with other studies, since our study deals with rolled sheets with highly anisotropic grain shape. The direction of microhardness indentation is the transversal direction of the sheets and the stress field of the compression by the indenter is three-dimensional, whereas the tensile test in our campaign loads the sample unidirectional along rolling direction. Therefore, the proportionality factor might change when the direction of microhardness or tensile load changes. Nevertheless, the obtained factor of 3.1 is very close to literature data and since tungsten does not show a strong hardening behaviour (as also seen in the  $\sigma$ - $\epsilon$  curves in Fig. 2), lower values around 3 are to be expected. In comparison, e.g. some materials with high work-hardening rate show proportionality factors of more than 4 [51].

From these observations, the following conclusions can be drawn: First, the correlation of UTS to microhardness (Fig. 7b) indicates that the rolling steps up to the second highest degree of deformation lead to a comparable increase in UTS and hardness, as the relation between both is linear and the proportionality factor of 3.1 is comparable to results in literature. Second, we discussed

above the influence of errors in the boundary spacing as a possible reason for the deviation of the sheets with highest degree of deformation. However, this deviation is not only seen in the Hall-Petch relations (Fig. 7a), but also seen in the correlation between UTS and Vickers hardness (Fig. 7b), where the boundary spacing is not explicitly incorporated. This further proves, that the enhanced increase in UTS and hardness with degree of deformation is not related to a resolution problem in the determination of the boundary spacing, but a real property of the material.

Up to now, we can only speculate about the reasons for this observation. A contributing factor for such an increase in hardness and UTS could be for example an increased dislocation density. An increasing amount of dislocation debris and forest dislocations restrict the motion of other dislocations and lead to strengthening. Therefore, measurements of dislocation density could prove useful which are, however, hard to quantify. A first qualitative hint for an exceptionally high dislocation density in the thinnest sheets are given by the TEM images published in the preceding study (see Fig. 11 in [30]).

#### Differences between $W_{pure}$ and $W_K$

All investigated  $W_K$  samples show slightly higher values for UTS than their  $W_{pure}$  counterparts (Fig. 3). When the dependence on grain size is considered, this difference in UTS is much more subtle, but still observable for experiments with  $T_f$  above  $300 \text{ }^\circ\text{C}$  (Fig. 6).

This could be caused by a slight strengthening effect due to the presence of dispersed bubbles in the K-doped material and other impurities introduced by the doping process itself (e.g. Al and Si), which have not been removed completely during heat treatment. This strengthening effect is further indicated by TEM observations on dislocations, which are regularly found entangled around K-bubbles (e.g. see Fig. 13 in [30]). However, the difference between the UTS of both material sets when compared at the same grain size is rather small, as is the total volume of potassium bubbles (60 ppm K) and the amount of impurities measured by chemical analysis of the bulk material (below 30 ppm for Al, Si and O altogether [30]).

## Conclusions

In this work, the tensile properties and the brittle-to-ductile transition temperatures are investigated for pure and K-doped tungsten sheets with five different degrees of deformation, respectively (logarithmic strains of 1.6 to 4.7). The results are compared to each other on the basis of the Hall-Petch relation for the dependence on grain size, leading to the following conclusions:

- The thinnest tungsten sheets with 50  $\mu\text{m}$  thickness show an outstanding  $T_{\text{BDT}}$  with  $-80\text{ }^{\circ}\text{C}$  (193 K) for  $W_{\text{pure}}(4.7)$  and  $-100\text{ }^{\circ}\text{C}$  (173 K) for  $W_{\text{K}}(4.6)$ . The sheets performance during tensile tests with loading along the rolling direction are outstanding as well. The values for UTS (2790 MPa and 2970 MPa) and  $\sigma_{\text{YS}}$  (2720 MPa and 2860 MPa) are to our knowledge the highest values reported for rolled tungsten sheets so far.
- The slightly lower  $T_{\text{BDT}}$  of the cold-rolled K-doped sheets compared to the pure W sheets is related to a smaller grain size of the K-doped sheets. We suggest, based on observations from a previous study, that K-bubbles in the W matrix do not directly enhance grain refinement during rolling, but inhibit growth of grains during heating of the W sheets between rolling steps.
- In general, the  $T_{\text{BDT}}$  for both material sets is in a similar range for comparable degree of deformation, except for the thickest sheets. We suggest the much higher  $T_{\text{BDT}}$  of the  $W_{\text{K}}$  sheet compared to the  $W_{\text{pure}}$  sheet to be provoked by several tens of  $\mu\text{m}$  thick orientation bands observed in the  $W_{\text{K}}$  sheet, which contain solely LABs.
- The thinnest sheets show a deviation from the Hall-Petch relation with much higher UTS and microhardness as expected. We assume an increased dislocation density to be responsible for that.
- The  $W_{\text{K}}$  sheets show a slightly higher UTS compared to their  $W_{\text{pure}}$  counterparts at comparable degree of deformation. This is related to the finer grain size of the  $W_{\text{K}}$  sheets and can be rationalized through the Hall-Petch relation.

In general, these observations indicate that no disadvantage in tensile strength and brittle-to-ductile transition is to be expected when K-doping is used to inhibit recrystallization in tungsten. Although the thickest K-doped sheet has much higher  $T_{\text{BDT}}$  than the pure W sheet, we relate this effect not to the K-doping but to orientation bands, which should be avoided during production. However, further investigations are needed in order to understand the brittle behaviour of this specific sheet. The slight strengthening effect due to K-doping, as seen in the previous study from the microhardness, is much more subtle in tensile strength and only seen at test temperatures of 300  $^{\circ}\text{C}$  and above. These promising results further encourage the use of K-doped tungsten for example in fusion reactor environments, where resistance to recrystallization and a certain amount of structural integrity is needed.

## Declaration of Competing Interest

The authors declare that they have no known competing financial interests or personal relationships that could have appeared to influence the work reported in this paper.

## CRediT authorship contribution statement

**Philipp Lied:** Project administration, Conceptualization, Investigation, Formal analysis, Writing - original draft, Visualization, Writing - review & editing. **Wolfgang Pantleon:** Formal analysis, Writing - review & editing. **Carsten Bonnekoh:** Formal analysis, Writing - review & editing. **Simon Bonk:** Formal analysis, Writing - review & editing. **Andreas Hoffmann:** Investigation, Resources, Writing - review & editing. **Jens Reiser:** Conceptualization, Supervision,

Funding acquisition, Writing - review & editing. **Michael Rieth:** Supervision, Funding acquisition, Writing - review & editing.

## Acknowledgements

This work has been carried out within the framework of the EUROfusion Consortium and has received funding from the Euratom research and training programme 2014-2018 and 2019-2020 under grant agreement No 633053. The views and opinions expressed herein do not necessarily reflect those of the European Commission. The support of Siegfried Baumgärtner (KIT) and the tungsten supplier, PLANSEE SE (Reutte/Austria), is gratefully acknowledged.

## Data availability

The raw/processed data required to reproduce these findings cannot be shared at this time as the data also forms part of an ongoing study.

## References

- [1] M. Rieth, S.L. Dudarev, S.M. Gonzalez de Vicente, J. Aktaa, T. Ahlgren, S. Antusch, D.E.J. Armstrong, M. Balden, N. Baluc, M.-F. Barthe, W.W. Basuki, M. Batabyal, C.S. Becquart, D. Blagoeva, H. Boldyryeva, J. Brinkmann, M. Celino, L. Ciupinski, J.B. Correia, A. de Backer, C. Domain, E. Gaganidze, C. García-Rosales, J. Gibson, M.R. Gilbert, S. Giusepponi, B. Gludovatz, H. Greuner, K. Heinola, T. Hörschen, A. Hoffmann, N. Holstein, F. Koch, W. Krauss, H. Li, S. Lindig, J. Linke, C. Linsmeier, P. López-Ruiz, H. Maier, J. Matejcek, T.P. Mishra, M. Muhammed, A. Muñoz, M. Muzyk, K. Nordlund, D. Nguyen-Manh, J. Opschoor, N. Ordás, T. Palacios, G. Pintsuk, R. Pippan, J. Reiser, J. Triebel, S.G. Roberts, L. Rومانer, M. Rosiński, M. Sanchez, W. Schulmeyer, H. Traxler, A. Ureña, J.G. van der Laan, L. Veleva, S. Wahlberg, M. Walter, T. Weber, T. Weitkamp, S. Wurster, M.A. Yar, J.H. You, A. Zivelonghi, Recent progress in research on tungsten materials for nuclear fusion applications in Europe, *Journal of Nuclear Materials* 432 (2013) 482–500 <https://doi.org/10.1016/j.jnucmat.2012.08.018>.
- [2] W. Martienssen, H. Warlimont, *Springer handbook of condensed matter and materials data*, Springer, Heidelberg, 2006.
- [3] J. Reiser, J. Hoffmann, U. Jäntsch, M. Klimenkov, S. Bonk, C. Bonnekoh, M. Rieth, A. Hoffmann, T. Mrotzek, Ductilisation of tungsten (W): On the shift of the brittle-to-ductile transition (BDT) to lower temperatures through cold rolling, *International Journal of Refractory Metals and Hard Materials* 54 (2016) 351–369 <https://doi.org/10.1016/j.jrmhm.2015.09.001>.
- [4] J. Reiser, S. Wurster, J. Hoffmann, S. Bonk, C. Bonnekoh, D. Kiener, R. Pippan, A. Hoffmann, M. Rieth, Ductilisation of tungsten (W) through cold-rolling: R-curve behaviour, *International Journal of Refractory Metals and Hard Materials* 58 (2016) 22–33 <https://doi.org/10.1016/j.jrmhm.2016.03.006>.
- [5] J. Reiser, L. Garrison, H. Greuner, J. Hoffmann, T. Weingärtner, U. Jäntsch, M. Klimenkov, P. Franke, S. Bonk, C. Bonnekoh, S. Sicking, S. Baumgärtner, D. Bolich, M. Hoffmann, R. Ziegler, J. Konrad, J. Hohe, A. Hoffmann, T. Mrotzek, M. Seiss, M. Rieth, A. Möslang, Ductilisation of tungsten (W): Tungsten laminated composites, *International Journal of Refractory Metals and Hard Materials*. <https://doi.org/10.1016/j.jrmhm.2017.07.013>.
- [6] J. Reiser, J. Hoffmann, U. Jäntsch, M. Klimenkov, S. Bonk, C. Bonnekoh, A. Hoffmann, T. Mrotzek, M. Rieth, Ductilisation of tungsten (W): On the increase of strength AND room-temperature tensile ductility through cold-rolling, *International Journal of Refractory Metals and Hard Materials* 64 (2017) 261–278 <https://doi.org/10.1016/j.jrmhm.2016.10.018>.
- [7] C. Bonnekoh, A. Hoffmann, J. Reiser, The brittle-to-ductile transition in cold rolled tungsten: On the decrease of the brittle-to-ductile transition by 600 K to  $-65\text{ }^{\circ}\text{C}$ , *International Journal of Refractory Metals and Hard Materials* 71 (2018) 181–189 <https://doi.org/10.1016/j.jrmhm.2017.11.017>.
- [8] S. Bonk, J. Reiser, J. Hoffmann, A. Hoffmann, Cold rolled tungsten (W) plates and foils: Evolution of the microstructure, *International Journal of Refractory Metals and Hard Materials* (2016) 60 <https://doi.org/10.1016/j.jrmhm.2016.06.020>.
- [9] S. Bonk, J. Hoffmann, A. Hoffmann, J. Reiser, Cold rolled tungsten (W) plates and foils: Evolution of the tensile properties and their indication towards deformation mechanisms, *International Journal of Refractory Metals and Hard Materials* 70 (2018) 124–133 <https://doi.org/10.1016/j.jrmhm.2017.09.007>.
- [10] V. Nikolic, S. Wurster, D. Firneis, R. Pippan, Improved fracture behavior and microstructural characterization of thin tungsten foils, *Nuclear Materials and Energy* 9 (2016) 181–188 <https://doi.org/10.1016/j.nme.2016.06.003>.
- [11] J. Reiser, M. Rieth, A. Möslang, B. Dafferner, J. Hoffmann, T. Mrotzek, A. Hoffmann, D.E.J. Armstrong, X. Yi, Tungsten foil laminate for structural divertor applications – Joining of tungsten foils, *Journal of Nuclear Materials* 436 (2013) 47–55 <https://doi.org/10.1016/j.jnucmat.2013.01.295>.
- [12] J. Reiser, M. Rieth, A. Möslang, H. Greuner, D.E.J. Armstrong, T. Denk, T. Gränning, W. Hering, A. Hoffmann, J. Hoffmann, H. Leiste, T. Mrotzek, R. Pippan,

- W. Schulmeyer, T. Weingärtner, A. Zabernig, Tungsten (W) Laminate Pipes for Innovative High Temperature Energy Conversion Systems, *Advanced Engineering Materials* 17 (2015) 491–501 <https://doi.org/10.1002/adem.201400204>.
- [13] F.J. Humphreys, A.D. Rollett, G.S. Rohrer, Recrystallization and related annealing phenomena, Elsevier, Amsterdam, 2017.
- [14] C. Bonnekoh, P. Lied, W. Pantleon, T. Karcher, H. Leiste, A. Hoffmann, J. Reiser, M. Rieth, The brittle-to-ductile transition in cold-rolled tungsten sheets: On the loss of room-temperature ductility after annealing and the phenomenon of 45° embrittlement (to be published, 2020).
- [15] E. Lassner, W.-D. Schubert, Tungsten - Properties, Chemistry, Technology of the Element, Alloys, and Chemical Compounds, Kluwer Academic, New York, 1999.
- [16] S. Antusch, J. Reiser, J. Hoffmann, A. Onea, Refractory Materials for Energy Applications, *Energy Technol* 5 (2017) 1064–1070 <https://doi.org/10.1002/ente.201600571>.
- [17] H.W. Deng, Z.M. Xie, Y.K. Wang, R. Liu, T. Zhang, T. Hao, X.P. Wang, Q.F. Fang, C.S. Liu, Mechanical properties and thermal stability of pure W and W-0.5 wt%ZrC alloy manufactured with the same technology, *Materials Science and Engineering: A* 715 (2018) 117–125 <https://doi.org/10.1016/j.msea.2017.12.112>.
- [18] P. Jenuš, A. Iveković, M. Kocen, A. Šestan, S. Novak, W2C-reinforced tungsten prepared using different precursors, *Ceramics International* 45 (2019) 7995–7999 <https://doi.org/10.1016/j.ceramint.2018.11.187>.
- [19] G. Leichtfried, Molybdenum lanthanum oxide: Special material properties by dispersoid refining during deformation, *Advances in Powder Metallurgy* 9 (1992) 123–138.
- [20] I. Wesemann, W. Spielmann, P. Heel, A. Hoffmann, Fracture strength and microstructure of ODS tungsten alloys, *International Journal of Refractory Metals and Hard Materials* 28 (2010) 687–691 <https://doi.org/10.1016/j.ijrmhm.2010.05.009>.
- [21] P. Schade, 100 years of doped tungsten wire, *International Journal of Refractory Metals and Hard Materials* 28 (2010) 648–660 <https://doi.org/10.1016/j.ijrmhm.2010.05.003>.
- [22] P. Schade, H.M. Ortner, I. Smid, Refractory metals revolutionizing the lighting technology: A historical review, *International Journal of Refractory Metals and Hard Materials* 50 (2015) 23–30 <https://doi.org/10.1016/j.ijrmhm.2014.11.002>.
- [23] M. Rieth, B. Dafferner, Limitations of W and W-1%La2O3 for use as structural materials, *Journal of Nuclear Materials* 342 (2005) 20–25 <https://doi.org/10.1016/j.jnucmat.2005.03.013>.
- [24] M. Fukuda, S. Nogami, A. Hasegawa, H. Usami, K. Yabuuchi, T. Muroga, Tensile properties of K-doped W-3%Re, *Fusion Engineering and Design* 89 (2014) 1033–1036 <https://doi.org/10.1016/j.fusengdes.2014.02.062>.
- [25] B. Gludovatz, S. Wurster, A. Hoffmann, R. Pippin, Fracture toughness of polycrystalline tungsten alloys 28 (2010). <https://doi.org/10.1016/j.ijrmhm.2010.04.007>.
- [26] V. Nikolić, J. Riesch, M.J. Pfeiferberger, R. Pippin, The effect of heat treatments on pure and potassium doped drawn tungsten wires: Part II – Fracture properties, *Materials Science and Engineering: A*. <https://doi.org/10.1016/j.msea.2018.09.029>.
- [27] V. Nikolić, J. Riesch, R. Pippin, The effect of heat treatments on pure and potassium doped drawn tungsten wires: Part I - Microstructural characterization, *Materials Science and Engineering: A*. <https://doi.org/10.1016/j.msea.2018.09.027>.
- [28] J. Riesch, Y. Han, J. Almanstötter, J.W. Coenen, T. Hörschen, B. Jasper, P. Zhao, C. Linsmeier, R. Neu, Development of tungsten fibre-reinforced tungsten composites towards their use in DEMO—potassium doped tungsten wire, *Physica Scripta T167* (2016) 14006 <https://doi.org/10.1088/0031-8949/T167/1/014006>.
- [29] M. Fukuda, S. Nogami, K. Yabuuchi, A. Hasegawa, T. Muroga, Anisotropy in the Mechanical Properties of Potassium and Rhenium Doped Tungsten Alloy Plates for Fusion Reactor Applications, *Fusion Science and Technology* 68 (2015) 690–693 <https://doi.org/10.13182/FST14-998>.
- [30] P. Lied, C. Bonnekoh, W. Pantleon, M. Stricker, A. Hoffmann, J. Reiser, Comparison of K-doped and pure cold-rolled tungsten sheets: As-rolled condition and recrystallization behaviour after isochronal annealing at different temperatures, *International Journal of Refractory Metals and Hard Materials* (2019) 105047 <https://doi.org/10.1016/j.ijrmhm.2019.105047>.
- [31] S. Nogami, S. Watanabe, J. Reiser, M. Rieth, S. Sickinger, A. Hasegawa, Improvement of impact properties of tungsten by potassium doping, *Fusion Engineering and Design* 140 (2019) 48–61 <https://doi.org/10.1016/j.fusengdes.2019.01.130>.
- [32] J. Reiser, M. Rieth, B. Dafferner, A. Hoffmann, Tungsten foil laminate for structural divertor applications – Basics and outlook, *Journal of Nuclear Materials* 423 (2012) 1–8 <https://doi.org/10.1016/j.jnucmat.2012.01.010>.
- [33] U.M. Ciucani, A. Thum, C. Devos, W. Pantleon, Isothermal annealing of thin rolled tungsten plates in the temperature range from 1300 °C to 1400 °C, *Nuclear Materials and Energy* 15 (2018) 128–134 <https://doi.org/10.1016/j.nme.2018.03.009>.
- [34] E08 Committee, E399: Standard Test Method for Linear-Elastic Plane-Strain Fracture Toughness K<sub>IC</sub> of Metallic Materials, ASTM International, West Conshohocken, PA.
- [35] C. Bonnekoh, J. Reiser, A. Hartmaier, S. Bonk, A. Hoffmann, M. Rieth, The brittle-to-ductile transition in cold-rolled tungsten sheets: the rate-limiting mechanism of plasticity controlling the BDT in ultrafine-grained tungsten, *J Mater Sci*. <https://doi.org/10.1007/s10853-020-04801-5>.
- [36] Y. Murakami, Stress intensity factors handbook, Pergamon, Oxford, 1987.
- [37] E28 Committee, E8/E8M: Standard Test Methods for Tension Testing of Metallic Materials, ASTM International, West Conshohocken, PA.
- [38] DIN, Deutsches Institut für Normung, Metallic materials – Tensile testing – Part 1: Method of test at room temperature.
- [39] F.B. Pickering, Physical Metallurgy and the Design of Steels (1978) 60.
- [40] I. Issa, A. Hohenwarter, R. Fritz, D. Kiener, Fracture properties of ultrafine grain chromium correlated to single dislocation processes at room temperature, *J. Mater. Res.* 34 (2019) 2370–2383 <https://doi.org/10.1557/jmr.2019.140>.
- [41] M. Hillert, On the theory of normal and abnormal grain growth, *Acta Metallurgica* 13 (1965) 227–238 [https://doi.org/10.1016/0001-6160\(65\)90200-2](https://doi.org/10.1016/0001-6160(65)90200-2).
- [42] C.L. Briant, O. Horacek, K. Horacek, The effect of wire history on the coarsened substructure and secondary recrystallization of doped tungsten, *Metallurgical Transactions A* 24 (1993) 843–851 <https://doi.org/10.1007/BF02656505>.
- [43] C.L. Briant, F. Zaverl, W.T. Carter, The effect of deformation on abnormal grain growth in tungsten ingots, *Acta Metallurgica et Materialia* 42 (1994) 2811–2821 [https://doi.org/10.1016/0956-7151\(94\)90222-4](https://doi.org/10.1016/0956-7151(94)90222-4).
- [44] Q. Wei, L.J. Kecskes, Effect of low-temperature rolling on the tensile behavior of commercially pure tungsten, *Materials Science and Engineering: A* 491 (2008) 62–69 <https://doi.org/10.1016/j.msea.2008.01.013>.
- [45] P. Zhao, J. Riesch, T. Hörschen, J. Almanstötter, M. Balden, J.W. Coenen, R. Himml, W. Pantleon, U. von Toussaint, R. Neu, Microstructure, mechanical behaviour and fracture of pure tungsten wire after different heat treatments, *International Journal of Refractory Metals and Hard Materials* 68 (2017) 29–40 <https://doi.org/10.1016/j.ijrmhm.2017.06.001>.
- [46] K. Sasaki, K. Yabuuchi, S. Nogami, A. Hasegawa, Effects of temperature and strain rate on the tensile properties of potassium-doped tungsten, *Journal of Nuclear Materials* 461 (2015) 357–364 <https://doi.org/10.1016/j.jnucmat.2015.03.015>.
- [47] G. Gottstein, Physical foundations of materials science, Springer Science & Business Media, 2013.
- [48] DIN, Deutsches Institut für Normung, DIN EN ISO 6507-1 Metallic materials - Vickers hardness test - Part 1: Test method.
- [49] D. Tabor, A Simple Theory of Static and Dynamic Hardness, *Proceedings of the Royal Society of London. Series A, Mathematical and Physical Sciences* 192 (1948) 247–274.
- [50] E28 Committee, E92: Test Methods for Vickers Hardness and Knoop Hardness of Metallic Materials, ASTM International, West Conshohocken, PA.
- [51] E.J. Pavlina, C.J. van Tyne, Correlation of Yield Strength and Tensile Strength with Hardness for Steels, *Journal of Materials Engineering and Performance* 17 (2008) 888–893 <https://doi.org/10.1007/s11665-008-9225-5>.